Electronic Supplementary Material (ESI) for Materials Advances.
This journal is © The Royal Society of Chemistry 2023

Solution-Processable Thin-Film Transistors from Anthradithiophene (ADT) and Naphthothiopene (NT) Small Molecule-Based p-Type Organic Semiconductors

Andrea Nitti,[a†] Mattia Scagliotti,[b†] Luca Beverina,[c] Luigi Mariucci,[b] Matteo Rapisarda[b*] and Dario Pasini[a*]

† Equal contribution

Table of contents

1. Synthesis

General Experimental. All commercially available reagents and solvents were purchased from Sigma-Aldrich, Fluorochem and Alfa Aesar. They were all used as received. Compounds **1**, **5a** and **5b** prepared according to literature procedures.[S1,S2] Flash chromatography was carried out using Merck silica gel 60 (pore size 60 Å, 270-400 Mesh). ^{1}H and ^{13}C NMR spectra were recorded from solutions in deuterated solvents on 300 Bruker or 400 Jeol spectrometers with the residual solvent as the internal standard.

Mass spectra of pure compounds were recorded using a Bruker Autoflex MALDI-TOF in positive reflectron mode with or without trans-2-(3-(4-tert-Butylphenyl)-2-methyl-2-propenylidene)malononitrile (DCTB) as the matrix. The spectra were recorded also without the matrix, giving in most cases equivalent results due to the direct formation of the radical cation of the relevant species.

Compound 3. Compound **3** was synthesized following an improved procedure with respect to that reported in literature.[S1] 9-(iodomethyl)nonadecane **2** (12.25 g, 30 mmol, 3 eq) was added to a solution of compound **1** (3.78 g, 10 mmol, 1 eq), Bu_4NI (3.69 g, 10 mmol, 1 eq), K_2CO_3 (4.15 g, 30 mmol, 3 eq) in dry DMAc (100 mL, 0.1 M) under inert atmosphere and then stirred at 80 °C for 48 h. After removal of solvent under reduced pressure, the reaction crude was dissolved in DCM (100 mL) and washed three times with a solution of NaOH 1M (10 mL total). The organic phase was concentrated under reduced pressure and precipitated in ^{i}PrOH (twice, 90 mL total) to give **3** as a yellow powder (6.85 g, 73%). ^{1}H NMR (400 MHz, $CDCl_3$) δ: 8.79 (s, 2H), 8.69 (s, 2H), 8.36 (d, J = 5.3 Hz, 2H), 7.63 (d, J = 5.3 Hz, 2H), 4.39 (d, J = 5.1 Hz, 4H), 1.92 (s, 2H), 1.57 – 1.13 (m, 64H), 0.95 – 0.75 (m, 12H). ^{13}C NMR (75 MHz, $CDCl_3$) δ: 166.6, 139.1, 134.6, 130.9, 130.0, 128.6, 126.6, 125.7, 125.2, 124.6, 77.2, 76.7, 76.3, 67.8, 37.3, 31.6, 31.4, 29.8, 29.4, 29.4, 29.3, 29.1, 26.6, 22.4, 13.8.

Compound 4a. Compound **4a** was synthesized following an improved procedure with respect to that reported in literature.[S1] A solution of compound **3** (1 g, 1.06 mmol, 1eq) in dry THF (25 mL) under argon was cooled to –40 °C with acetonitrile/CO_2(s) bath. After 15 min, a solution of LDA (1 M in hexane, 4.26 mL, 4.26 mmol, 3 eq) was added dropwise, than the red dark mixture was cooled to –78 °C and kept for 2 h at the same temperature. After that, Bu_3SnCl (722 µL, 2.66 mmol, 2.5 eq) was added in one portion. The reaction mixture was kept at –78°C for 30 min, and then it was warmed to room temperature and stirred overnight. The reaction mixture was quenched with H_2O (20 mL) and the organic solvent was removed under reduced pressure. The aqueous phase was extracted with Et_2O (3 × 20 mL), than the combined organic phase was dried (Na_2SO_4) and solvent removed under

reduced pressure. Reaction crude was purified by short flash chromatography on neutral alumina (*n*-hexane as the eluent) affording **4a** as a pale yellow oil (1.31 g, 94%). The spectroscopic data were coherent with literature.

*General procedure for the synthesis of compounds **6–8** by Stille cross-coupling.*[2,3] *Synthesis of compound* **6**. A solution of compound **4a** (303 mg, 0.2 mmol, 1 eq), compound **5b** (235 mg, 0.4 mmol, 2 eq) in dry toluene (2 mL) was degassed for 5 min under argon atmosphere. $Pd(PPh_3)_4$ (4.62 mg, 0.004 mmol, 0.02 eq) was added in one portion, and the solution was further degassed for 10 min. The reaction mixture was heated at reflux under stirring for 24 h. The reaction solvent was removed under reduced pressure and the reaction mixture was purified by flash chromatography (SiO_2; petroleum ether:DCM 8:2), to obtain compound **6** as a dark yellow solid (277 mg, 71%).

Compound **6**. Dark yellow solid (277 mg, 71%). ^{1}H NMR (400 MHz, $CDCl_3$) δ: 8.40 (s, 2H), 8.28 (s, 2H), 8.20 (s, 2H), 8.18 (s, 2H), 8.13 (s, 2H), 7.74 (d, J = 8.0 Hz, 4H), 7.62 (d, J = 8.0 Hz, 4H), 7.39 (t, J = 7.4 Hz, 4H), 7.25 (t, J = 7.4 Hz, 4H), 4.52 (d, J = 5.0 Hz, 4H), 4.44 (d, J = 5.4 Hz, 4H), 2.12 – 2.02 (m, 2H), 1.98 (d, J = 5.3 Hz, 2H), 1.66 – 1.13 (m, 128H), 0.82 (dd, J = 12.9, 6.0 Hz, 24H). ^{13}C NMR (101 MHz, $CDCl_3$) δ: 166.3, 166.1, 138.3, 138.2, 137.2, 137.1, 135.7, 134.7, 131.0, 130.4, 130.1, 129.5, 129.4, 128.6, 127.3, 125.8, 124.4, 124.2, 123.7, 123.3, 123.2, 123.0, 68.5, 68.2, 37.8, 32.1, 32.1, 32.1, 31.9, 31.8, 30.4, 30.0, 29.9, 29.9, 29.8, 29.6, 29.5 27.2, 22.8, 22.8, 14.2. MALDI-TOF: $[M]^+$ = 1953.

Compound **7**. Dark yellow solid (306 mg, 71%). ^{1}H NMR (400 MHz, $CDCl_3$) δ: 8.46 – 7.90 (m, 6H), 7.59 (m, 6H), 7.41 – 6.86 (m, 6H), 4.52 (m, 8H), 2.20 – 1.91 (m, 6H), 1.90 – 1.08 (m, 94H), 1.16 – 0.63 (m, 18H). ^{13}C NMR (101 MHz, $CDCl_3$) δ: 166.3, 166.1, 138.3, 138.2, 137.2, 137.1, 135.7, 134.7, 131.0, 130.4, 130.1, 129.5, 129.4, 128.6, 127.3, 125.8, 124.4, 124.2, 123.7, 123.3, 123.2, 123.0, 68.5, 68.2, 37.8, 32.1, 32.1, 32.1, 31.9, 31.8, 30.4, 30.0, 29.9, 29.9, 29.8, 29.6, 29.5 27.2, 22.8, 22.8, 14.2. MALDI-TOF *m/z*: $[M]^+$ Calcd for $C_{102}H_{134}O_8S_4$ 1614.8962; Found 1614.7048.

Compound **8**. Dark yellow solid (301 mg, 70%). ^{1}H NMR (400 MHz, $CDCl_3$) δ: 8.46 (s, 2H), 8.41 (s, 2H), 8.01 (d, J = 8.1 Hz, 2H), 7.87 (d, J = 8.5 Hz, 2H), 7.81 (d, J = 2.8 Hz, 2H), 7.61 (t, J = 7.6 Hz, 2H), 7.47 (t, J = 7.4 Hz, 2H), 7.38 (d, J = 3.4 Hz, 2H), 7.01 (d, J = 3.5 Hz, 2H), 4.37 (d, J = 5.6 Hz, 4H), 3.03 (t, J = 7.9 Hz, 4H), 1.98 – 1.83 (m, 7H), 1.60 – 1.17 (m, 104H), 0.93 (t, J = 6.6 Hz, 7H), 0.86 (t, J = 6.6 Hz, 14H). ^{13}C NMR (101 MHz, CDCl3) δ: 14.2, 14.3, 22.8, 22.8, 27.0, 29.5, 29.6, 29.6, 29.7, 29.8, 29.8, 30.1, 30.5, 31.7, 32.0, 32.1, 37.6, 68.2, 120.7, 123.4, 123.6, 123.7, 123.8, 124.5, 126.3, 128.2, 129.1, 129.8, 130.3, 130.5, 130.8, 135.9, 136.6, 137.3, 137.4, 138.2, 138.9, 139.1, 147.4, 166.7. MALDI-TOF *m/z*: $[M]^+$ Calcd for $C_{100}H_{134}O_4S_6$ 1590.8606; Found 1590.8591.

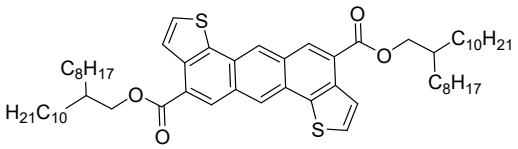

	Amount (g)	Waste (g)
Compound **1**	3.78	1.02
9-(iodomethyl)nonadecane	12.25	6.29
K_2CO_3	4.15	4.15
DMAc	94	0
DCM	100	0
NaOH 1M	10	10
iPrOH	90	90
Total	**314.18**	**111.46**

Total waste = 425.64 g; Compound obtained = 6.85 g

E-factor = 16

2. UV-vis and emission studies

UV-Visible spectra were collected by Perkin-Elmer Lambda900 spectrophotometer. The solid UV-Vis diffuse reflectance spectra were recorded using a Shimadzu UV3600 spectrophotometer with $BaSO_4$ as a reference. Steady state emission and excitation spectra were obtained using both a FLS 980 (Edinburg Instrument Ltd) and a Nanolog (Horiba Scientific) spectrofluorimeter. The spectra are corrected for the instrument response. PL Quantum Yields of solutions are obtained by using Rhodamine 6G as the reference. PL QY of solid-state samples were measured with a home-made integrating sphere according to the procedure reported elsewhere.[S3]

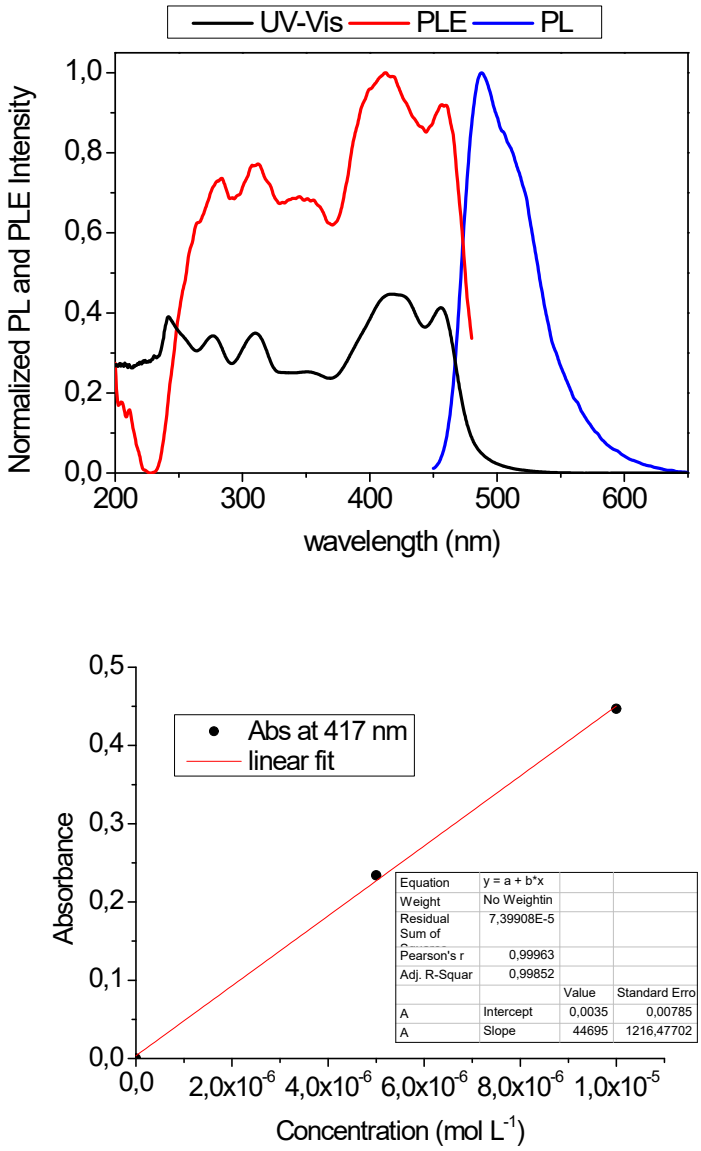

Figure S1. *Top:* UV-Vis (black), PLE (red) and PL (blue) spectra of compound **8** in dilute solution of $CHCl_3$ (10^{-6} M). *Bottom:* Calculation of molar absorptivity for compound **8**.

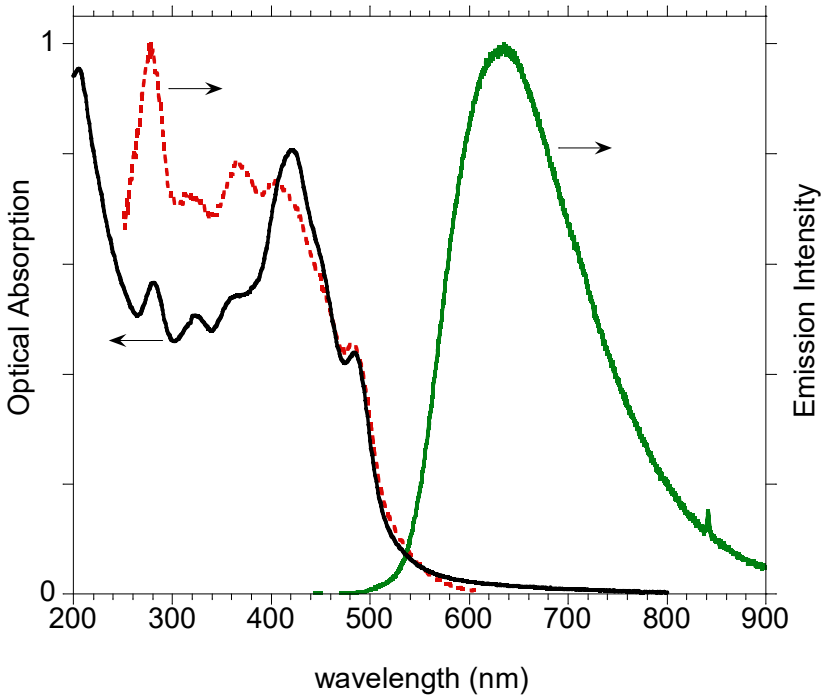

Figure S2. UV-Vis (black), PL (green) and PLE (red) spectra of compound **8** in film-cast.

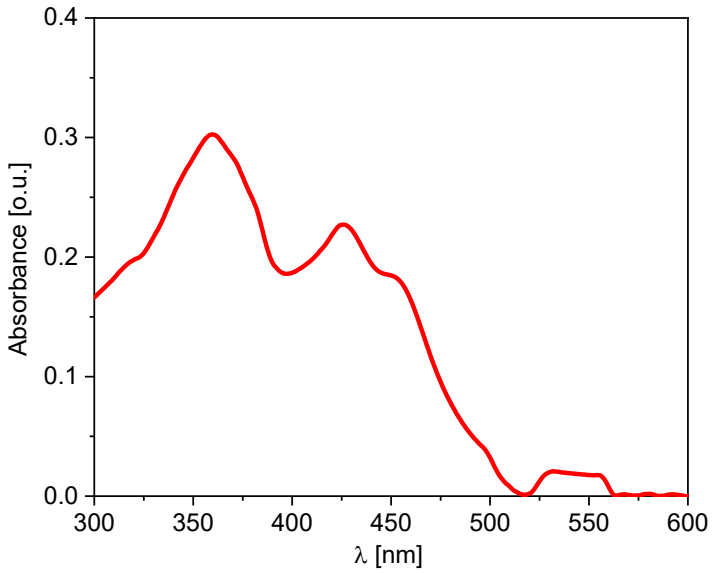

Figure S3. Absorption spectra of a film of compound **6** deposited on glass by spin coating from toluene solutions.

3. Cyclic Voltammetry

Cyclic voltammetry experiments were carried out using a Epsilon-Eclipse potentiostat with a polished glassy carbon working electrode, platinum counter electrode, silver pseudo-reference electrode, and tetrabutylammonium hexofluorophosphate (recrystallized three times from EtOH) as a supporting electrolyte. Sample concentrations were between 0.2 and 1.0 mM in DCM. All electrochemical measurements were referenced to the Fc/Fc^{+} redox couple. Band gaps were estimated using the onset of the initial oxidation and reduction events, and E_{HOMO} and E_{LUMO} were estimated given an E_{HOMO} of 4.80 eV for ferrocene. In all figures the first scan is shown, which is similar to subsequent scans.

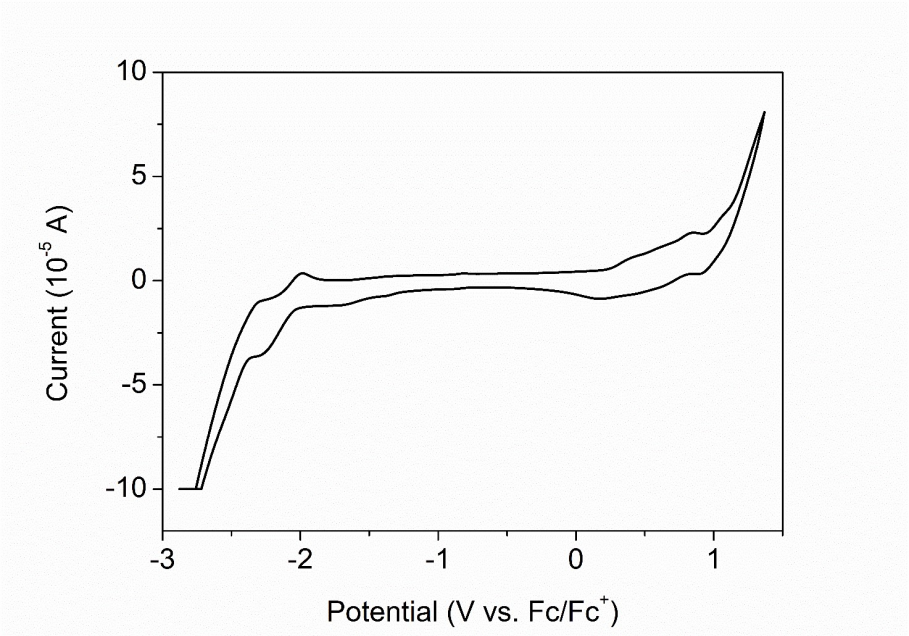

Figure S4. Cyclic voltammogram of compound **8**.

4. Devices Fabrication and Optimization

Figure S5 shows the two different types of OTFT device test structures fabricated and tested: bottom gate bottom contact (BGBC, Figure S5a) and bottom gate top contact (BGTC, Figure S5b) thin film transistors. We tested BGTC structures with two different gate dielectric layers: 1) 100 nm thick SiO_2 dielectric layer; 2) 100 nm thick SiO_2 layer with an additional layer of 300 nm of PMMA. In BGBC structures, after cleaning the substrate in acetone and isopropanol ultrasonic bath, the Source (S) and Drain (D) Au contacts were patterned using lithographic techniques and the organic semiconductor was deposited above them. In BGTC structures the semiconductor layer was deposited on the SiO_2 or PMMA layers. The 300 nm thick layer of polymethylmethacrylate (PMMA) has been deposited by spin-coating. The Source and Drain contacts were made as the last step of the manufacturing process by thermal evaporation in high vacuum and patterned by a shadow mask. The synthesized semiconductor materials have been dissolved in toluene with a concentration of 15 mg/ml and have been magnetic stirred for 18/24 hours under nitrogen atmosphere. The solution has been deposited by spin coating technique at 1500 rpm for 30 s which results in a film thickness of 30 nm. The as-fabricated devices have been electrically characterized using an MMR cryostat connected to a Keithley 236 and a Keithley 2635 source/meter units. The normalized transfer characteristics I_D L / W C_i of the different tested OTFT structures are shown in Figure S5c. C_i is the insulator capacitance per unit area ($C_i=\varepsilon_0\ \varepsilon_r/d$, where ε_0 is the vacuum permittivity, ε_r is the relative permittivity in the dielectric material and d is the dielectric thickness). Extracted C_i values are 5 $nFcm^{-2}$ for the BGTC PMMA+SiO_2 structure and 35 $nFcm^{-2}$ for the structure with only SiO_2 as dielectric layer. The I_D *vs* V_{GS} measurements were acquired in air sweeping up-down the gate voltage from off to on regime and then in the opposite way, as indicated by black arrows in the graphs. The measurements show a large increase in stability and performances of BGTC transistor compared to BGBC devices for both the BGTC structures. In particular, the top S&D electrodes configuration reduces the presence of contact effects occurring between the OSC and the S&D electrodes, by decreasing the defects at the interface and maintains an excellent interface region between the OSC layer and the dielectric, which is very important for the stability of the device characteristics. Between the top contact configurations, the devices with SiO_2/PMMA gate dielectric show better performances showing higher mobility values and reduced hysteresis compared to the OTFTs with SiO_2 gate dielectric. This suggests that the interface between PMMA and semiconductor is less defected as a result of an improved molecular structure at the dielectric/semiconductor interface. In Figure S1d the transfer curves of the optimized devices are reported in linear and log scale for V_{DS}=-1 V and V_{DS}=-20 V. In the inset is reported the maximum of the transconductance curve.

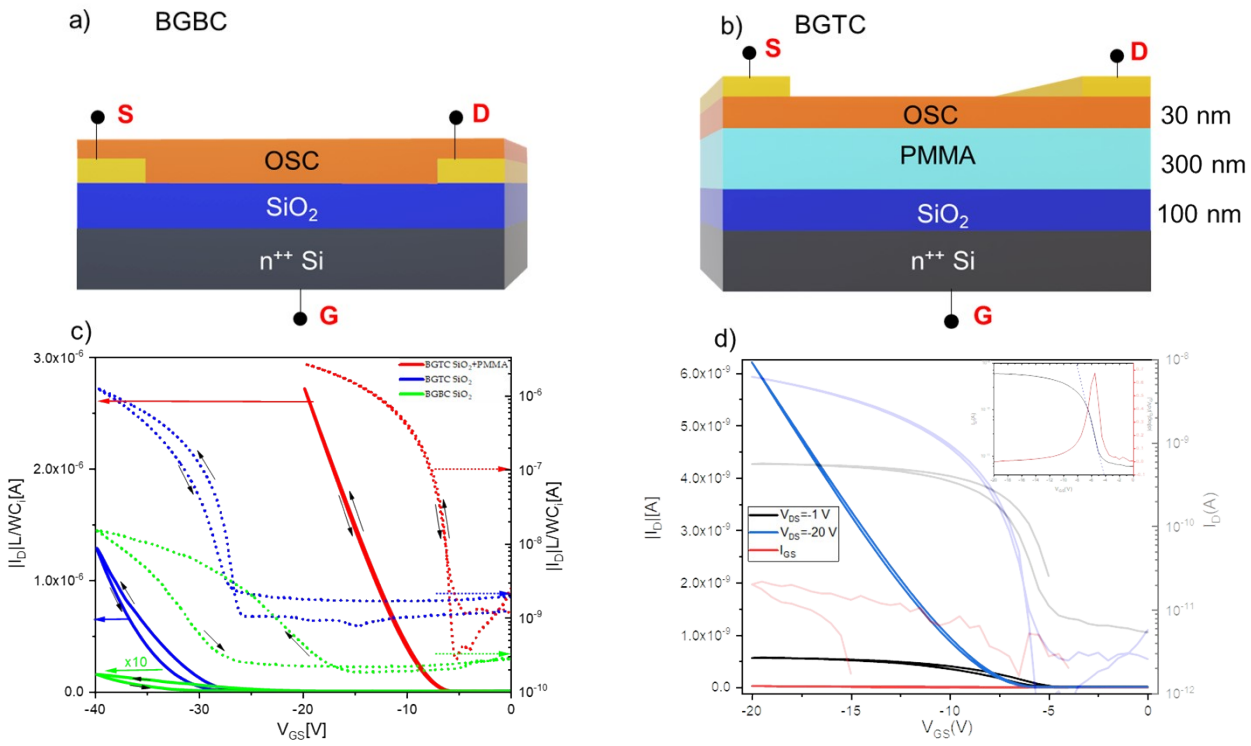

Figure S5. a) Bottom Gate Bottom Contact (BGBC) OTFT device realization scheme. The Source (S) and Drain (D) Au contacts were patterned using lithographic techniques and the organic semiconductor was deposited above them; b) Bottom Gate Top Contact (BGTC) OTFT device realization scheme. The S&D contacts were patterned using a shadow mask above the organic semiconductor layer; c) Comparison of the normalized up-down transfer characteristics I_D L / W C_i vs V_{GS} with V_{DS}= -20 V of devices, based on compound 6 and having the three different structures we tested. The continuous lines refer to the linear left scale while the dotted lines refer to the log right scale. For the green continuous line (BGBC structure) the value of the ordinate axis is multiplied by 10 (only for the linear left scale) to improve the graph visualization. d) I_D vs V_{GS} transfer characteristics of an optimized BGTC PMMA OTFT realized with Compound 6 as OSC layer.

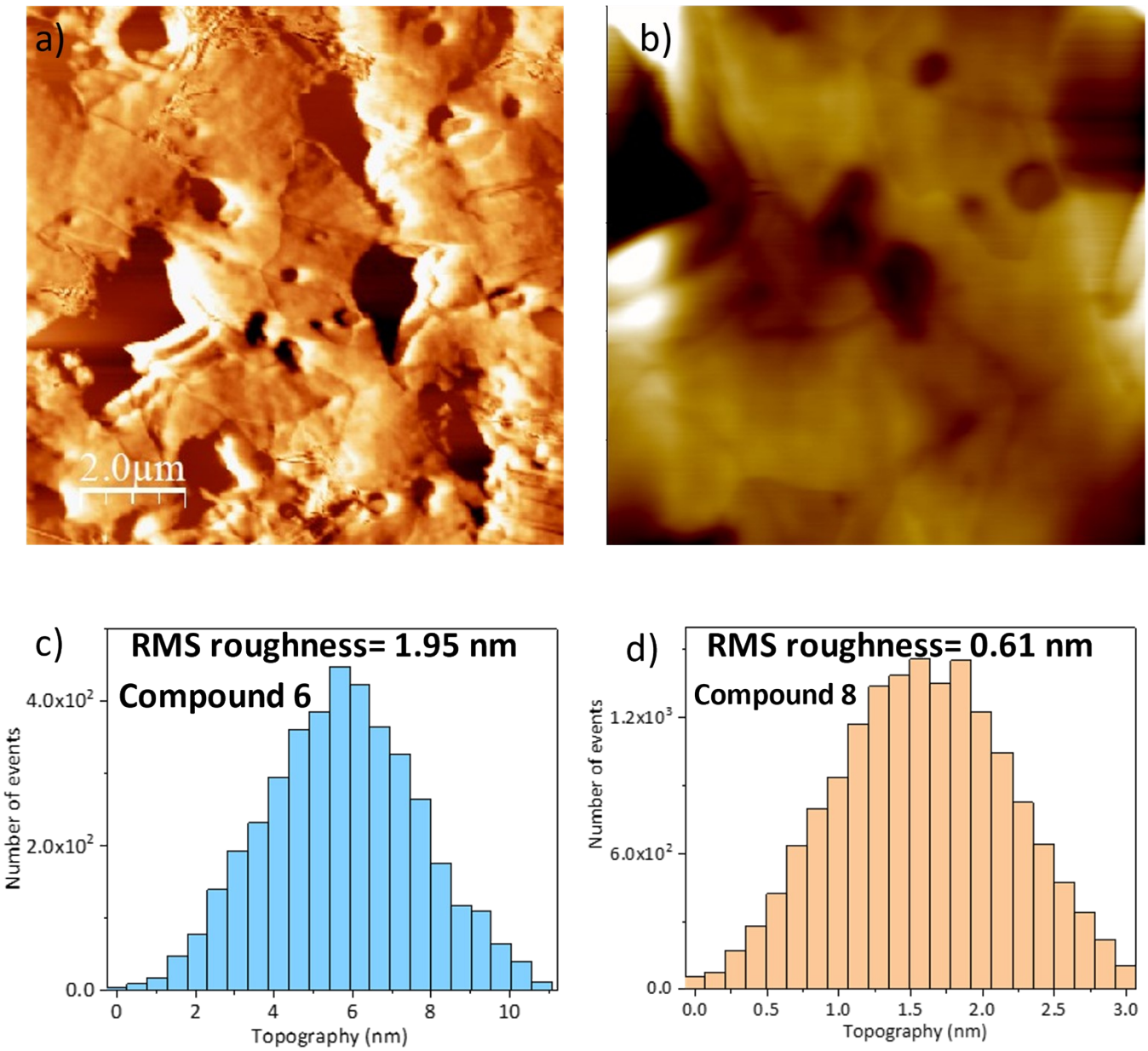

Figure S6. AFM error signal 10x10 µm a) and topography 5x5 µm b) images of compound **6** OTFT device; c)-d) RMS roughness calculation for compound **6** and Compound **8**.

5. Phototransistor performances

The Responsivity is the figure of merit of a photodetector which measures the electrical output per optical input. It is defined as

$$R = \frac{J_{light} - J_{dark}}{P_{opt}} = \frac{J_{ph}}{P_{opt}}$$

where J_{light} and J_{dark} are the current density (I_{ds}/active area) under illumination and in dark respectively. J_{ph} is the electrical output of the photodetector while P_{opt} is the incident optical power density and measures the optical input of the detector. In OPT devices, typically, the responsivity depends on the polarization voltages (V_{ds} and V_{gs}) during illumination, and the maximum R values are obtained in TFT saturation regime, at high V_{gs} [S4]. In the following table, OPT device presented in this work is compared in terms of responsivity with the most recent literature works that report OPTs made both on rigid and flexible substrates with different organic semiconductors and gate dielectrics. The measured R is comparable with the other works in particular for OPTs with polymeric gate dielectrics, showing that the presented material can be efficiently used in UV-Vis detection in OPT flexible devices.

Phototransistor structure	**Semiconductor**	**Semiconductor deposition technique**	**Dielectric layer**	**Investigated λ (nm)**	**R(A/W) max**	**Ref**
BGTC, L=50-500 μm	Compound 6 of this work (small molecule based on ADT and NT)	From solution	PMMA	450	**3.5** Vds=-20 V Vgs=-15 V	**This work**
BGTC L=100	DNTT	HV evaporation	Cytop	450	**150** Vds=Vgs= -25V	S4
TGBC	DPPT-TT/TFP:PS	From Solution	Cyanoresin (high-k)	250-1000	**0.091** Vds=-30 V	S5
BGTC	PODTPPD-BT (active layer), P3HT (channel layer)	From Solution	PMMA	200-1000 max at 780	**0.38** Vds=Vgs=-30 V	S6
TGBC	P3HT:PDPPTTT	From Solution	PMMA/PVA Low k/high-k	350-900	**2.43** (p-channel) Vgs=-30 V Vds=-40 V **4.29** (n-channel) Vgs=Vds=+40 V	S7
BGTC	PBIBDF-TT nanowire	From solution	SiO_2	400-1200, max at 808	**0.44** Vgs=Vds=-80 V	S8
BGTC	PDVT-8/PC61BM	From solution	SiO_2	720	**750** Vds=-40 V	S9
BGTC	PBIBDF-BT	From solution	OTS/SiO_2	600–1000, max at 650	**0.1** (p-channel) **0.04** (n-channel) Vds=-80 V	S10

6. NMR and mass spectra of new compounds

Compound **7**

^{1}H NMR ($CDCl_3$, 400 MHz)

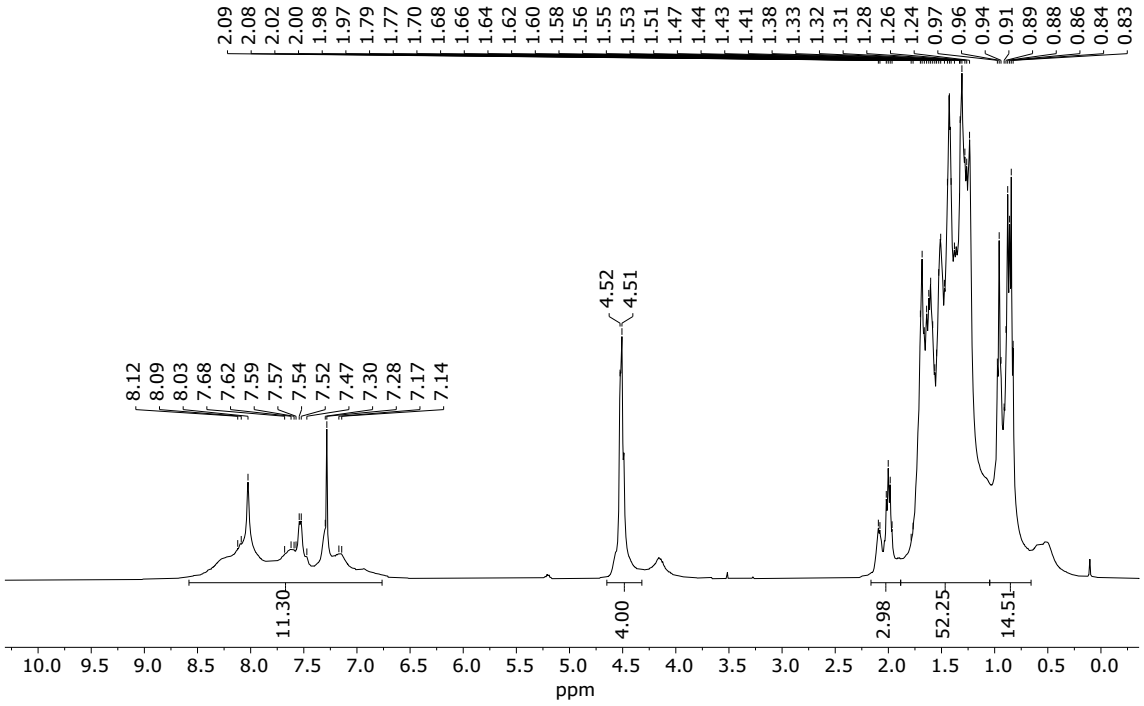

^{13}C NMR (400 MHz, $CDCl_3$)

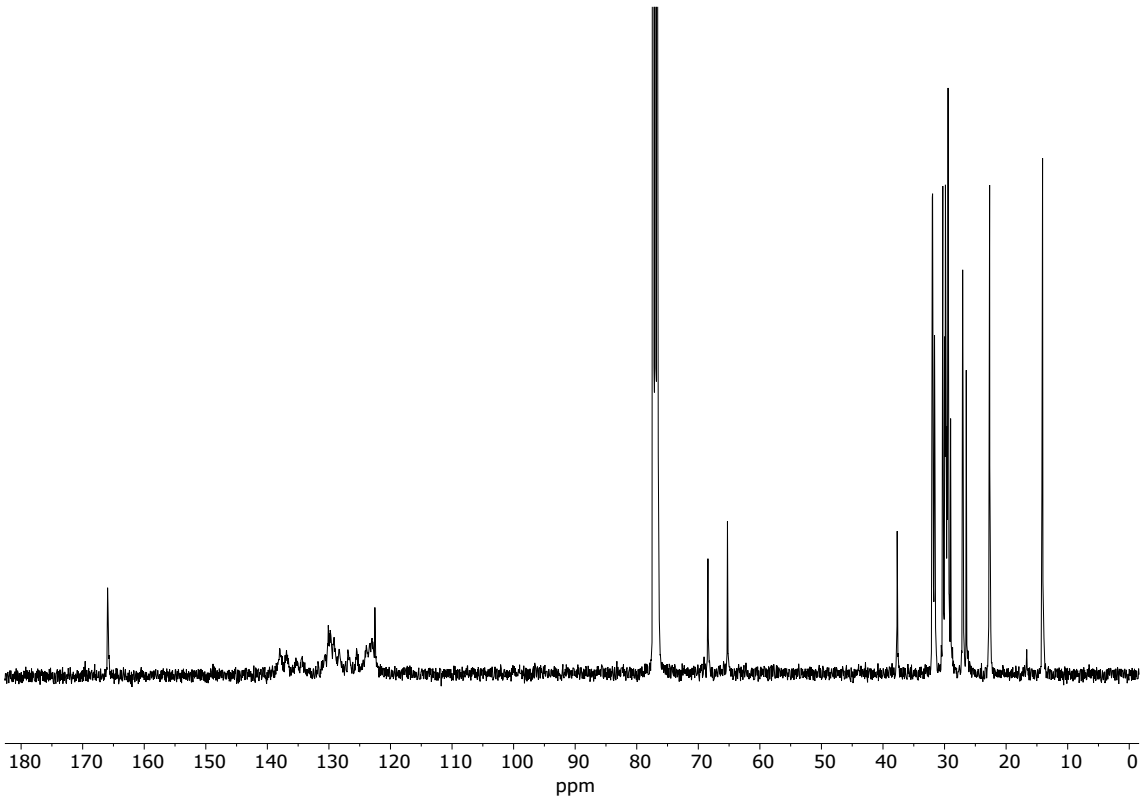

COSY

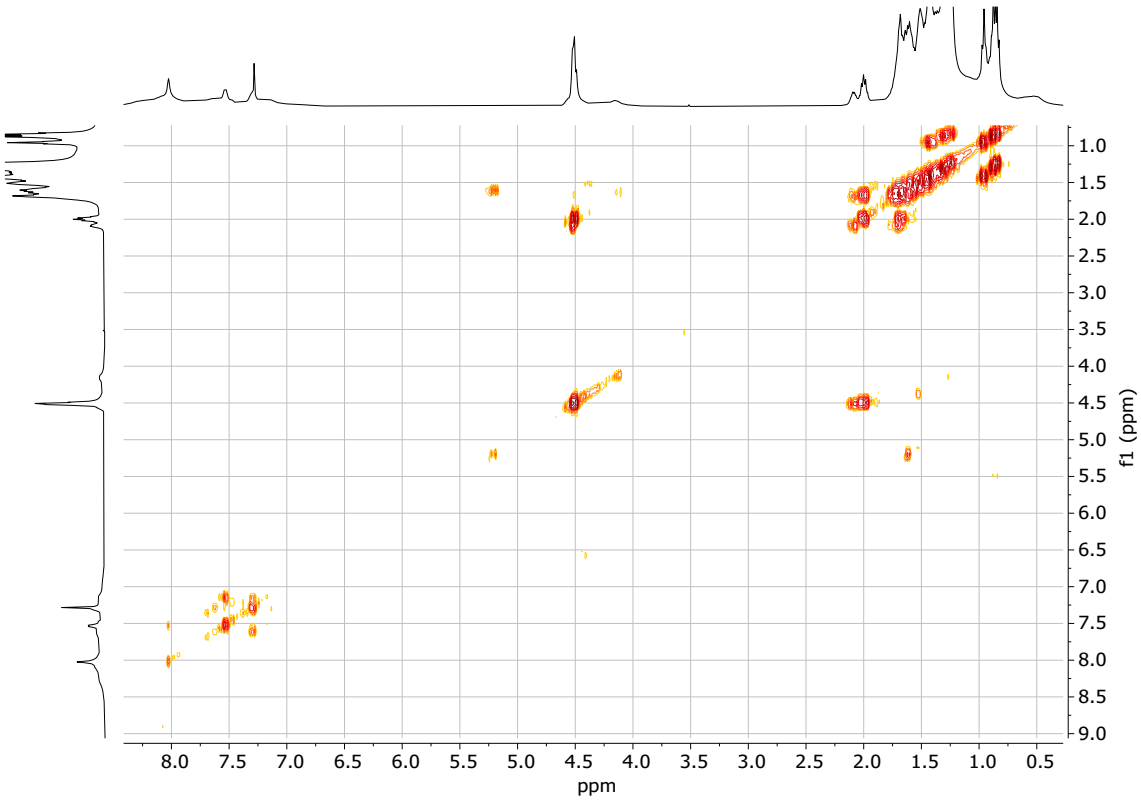
1.0
1.5
2.0
2.5
3.0
3.5
4.0
4.5
5.0
5.5
6.0
6.5
7.0
7.5
8.0
8.5
9.0
f1 (ppm)
8.0
7.5
7.0
6.5
6.0
5.5
5.0
4.5
4.0
3.5
3.0
2.5
2.0
1.5
1.0
0.5
ppm

HSQC

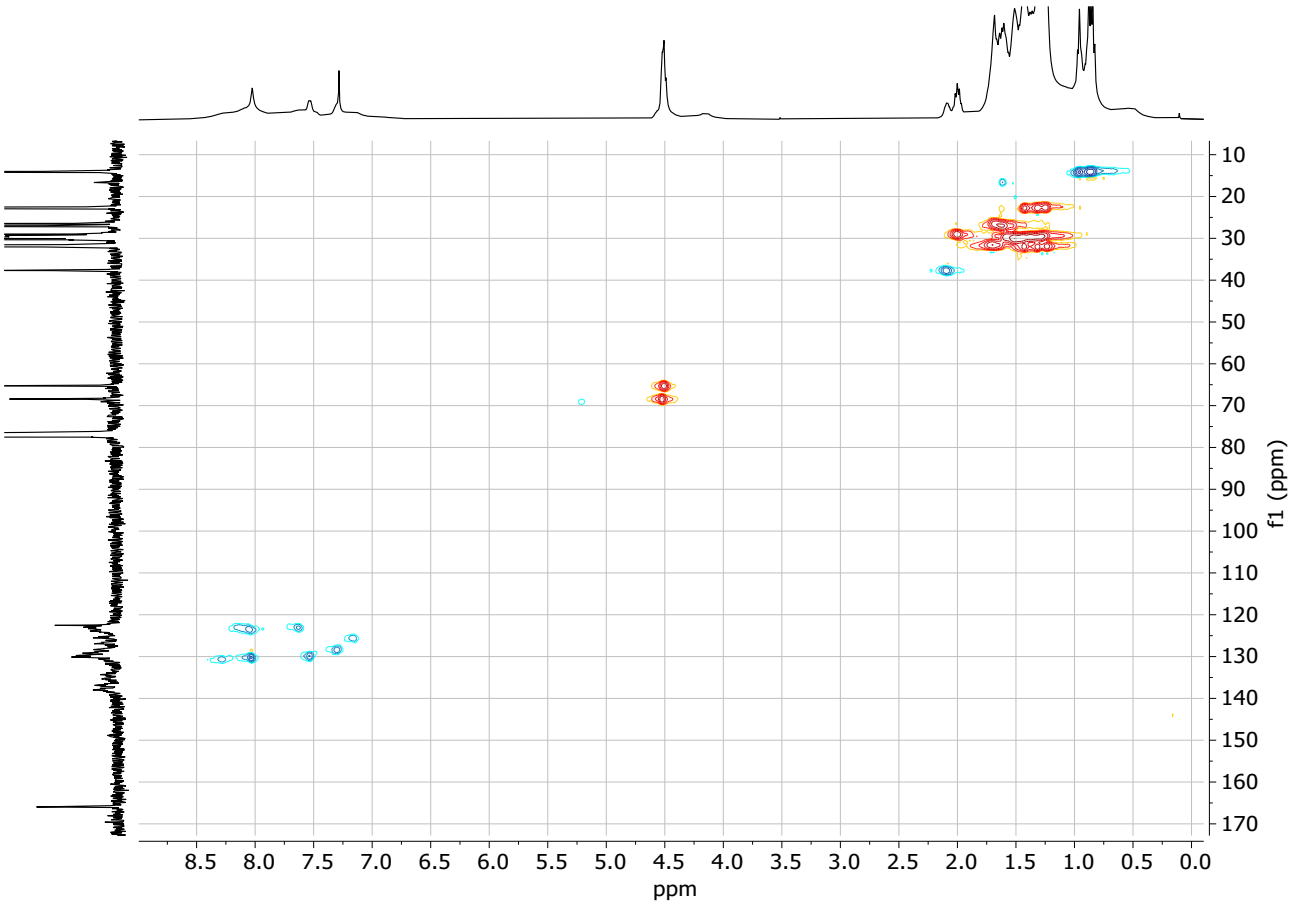
10
20
30
40
50
60
70
80
90
100
110
120
130
140
150
160
170
f1 (ppm)
8.5
8.0
7.5
7.0
6.5
6.0
5.5
5.0
4.5
4.0
3.5
3.0
2.5
2.0
1.5
1.0
0.5
0.0
ppm

MALDI-TOF

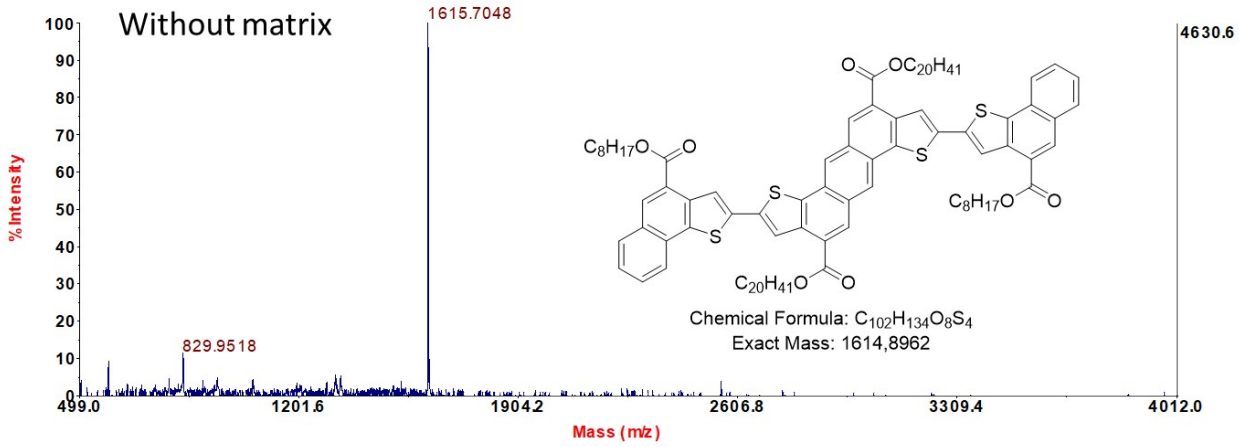
Without matrix
1615.7048
4630.6
829.9518
% Intensity
Mass (m/z)
499.0
1201.6
1904.2
2606.8
3309.4
4012.0
$C_8H_{17}O$
$OC_{20}H_{41}$
$C_{20}H_{41}O$
Chemical Formula: $C_{102}H_{134}O_8S_4$
Exact Mass: 1614,8962

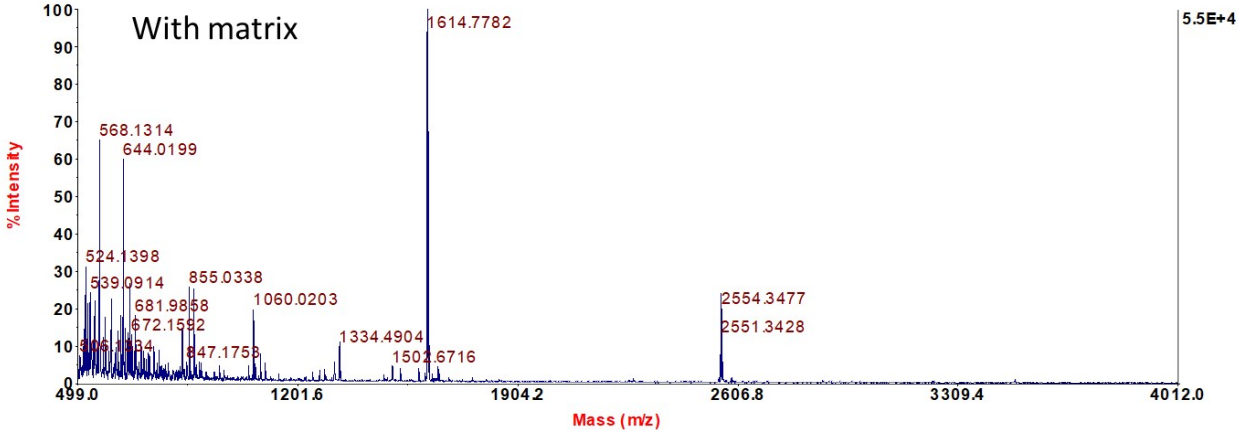
With matrix
1614.7782
5.5E+4
568.1314
644.0199
524.1398
539.0914
855.0338
1060.0203
681.9858
672.1592
1334.4904
847.1758
1502.6716
2554.3477
2551.3428
% Intensity
Mass (m/z)
499.0
1201.6
1904.2
2606.8
3309.4
4012.0

Compound **8**

^{1}H NMR ($CDCl_3$, 400 MHz)

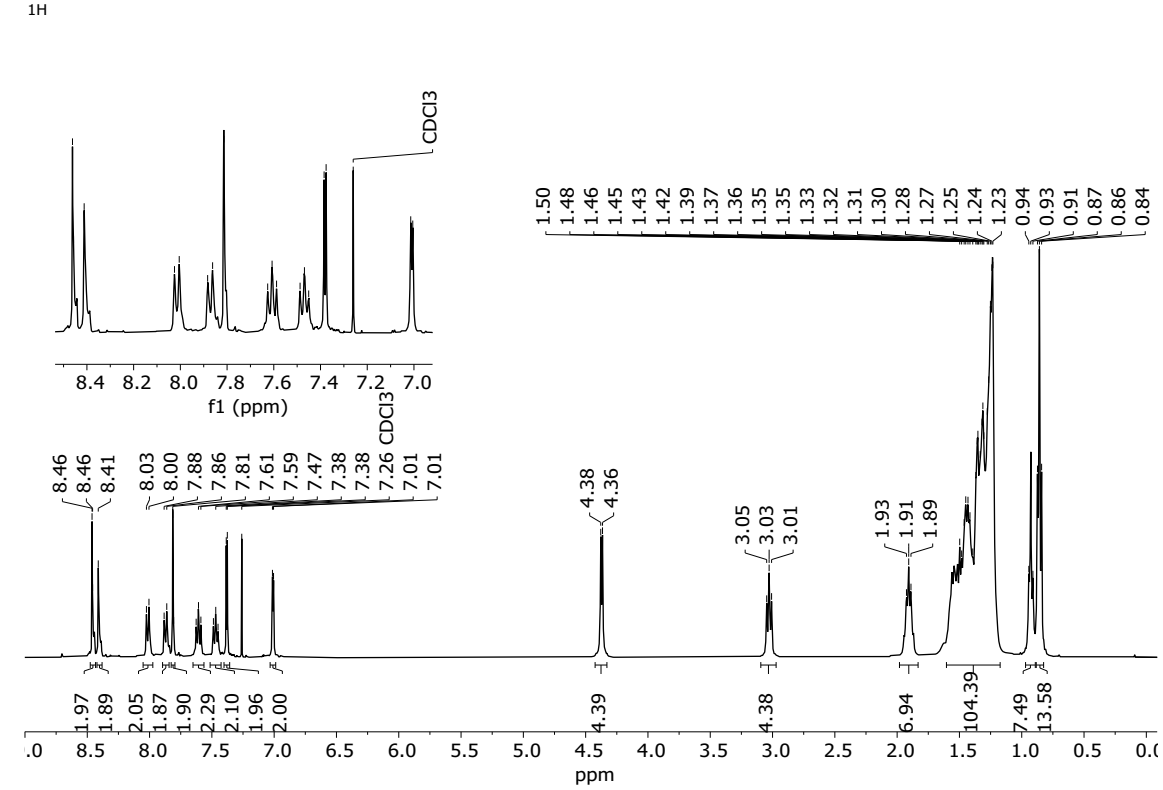

^{13}C NMR

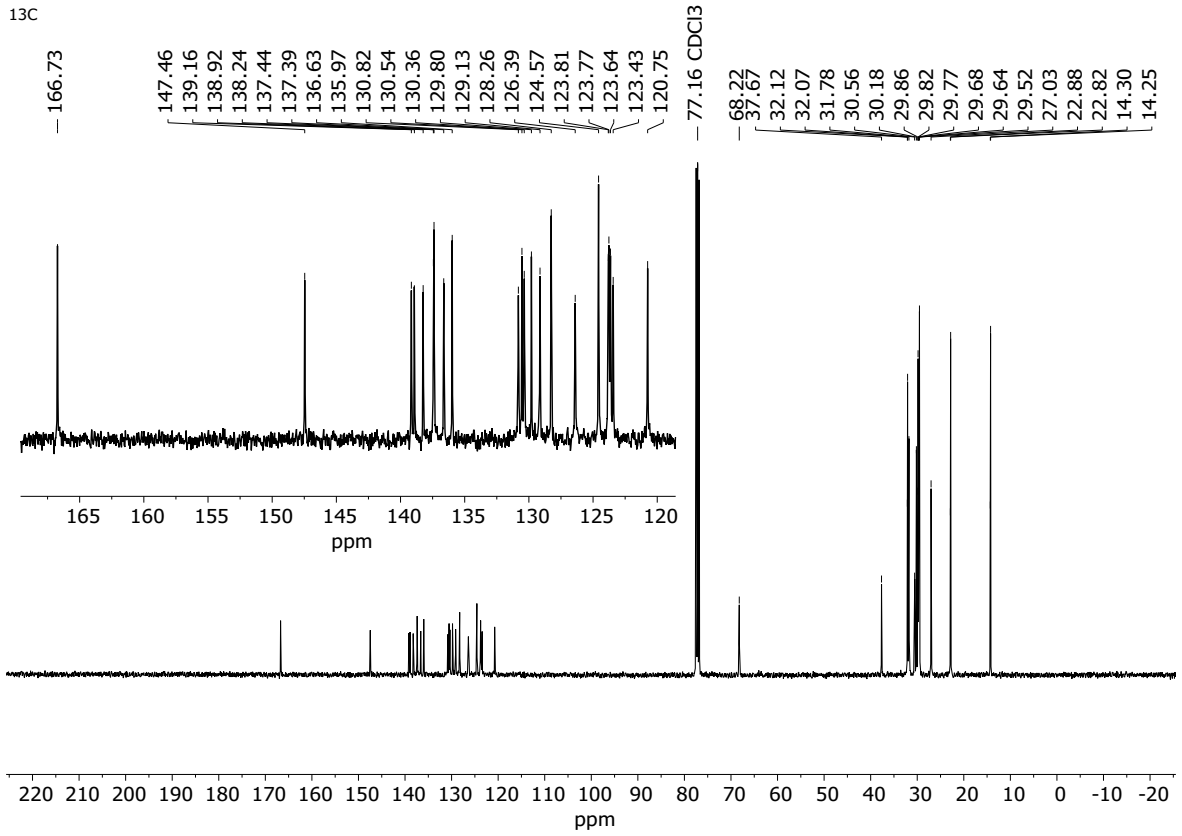

COSY

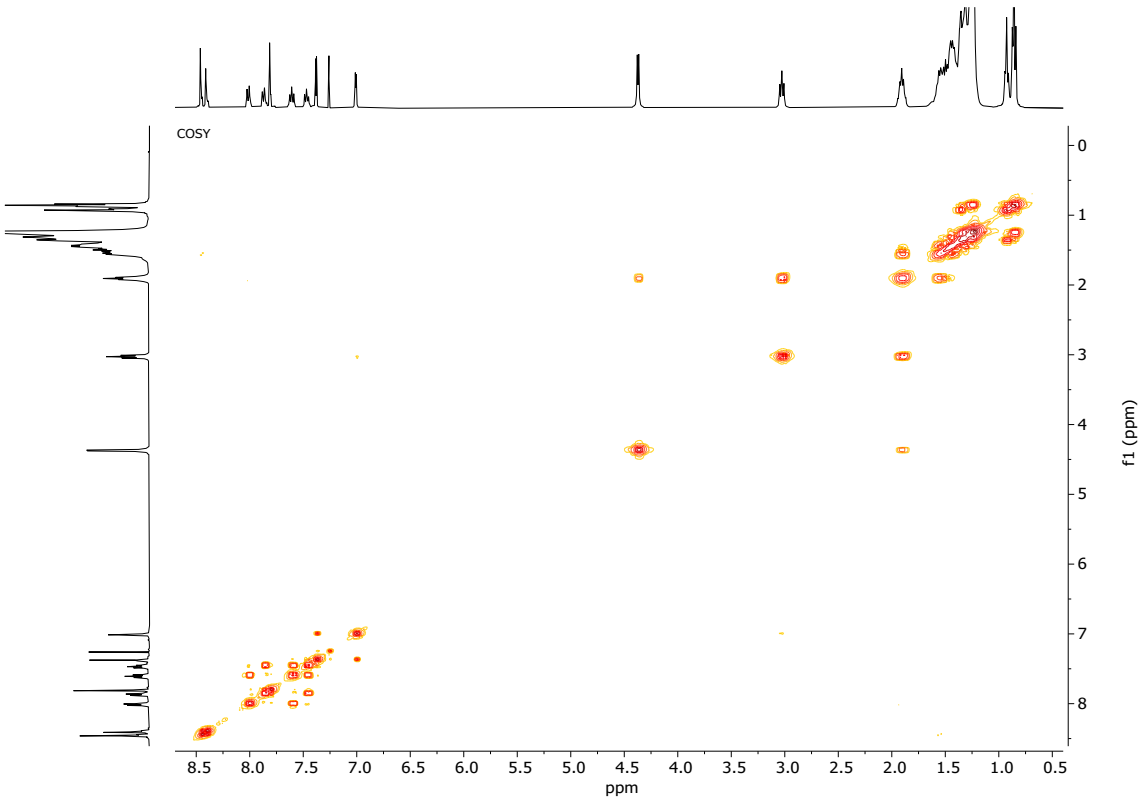
COSY
8.5 8.0 7.5 7.0 6.5 6.0 5.5 5.0 4.5 4.0 3.5 3.0 2.5 2.0 1.5 1.0 0.5
ppm
0 1 2 3 4 5 6 7 8
f1 (ppm)

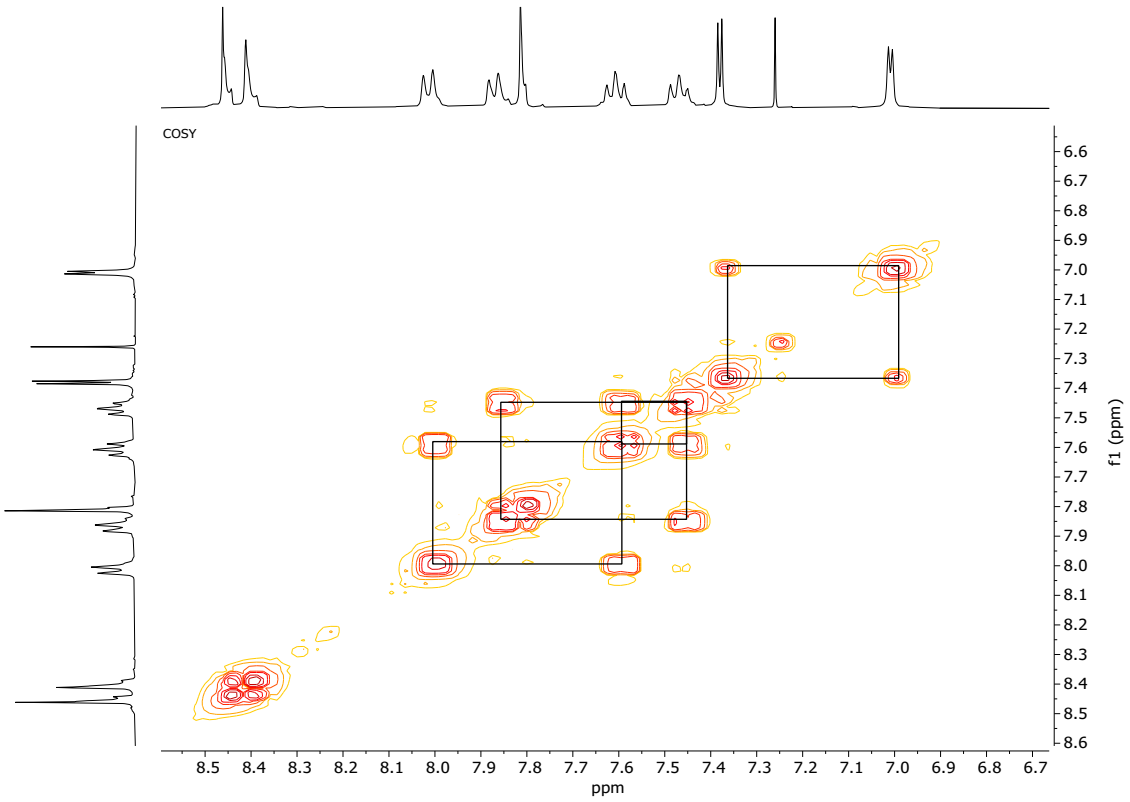
COSY
8.5 8.4 8.3 8.2 8.1 8.0 7.9 7.8 7.7 7.6 7.5 7.4 7.3 7.2 7.1 7.0 6.9 6.8 6.7
ppm
6.6 6.7 6.8 6.9 7.0 7.1 7.2 7.3 7.4 7.5 7.6 7.7 7.8 7.9 8.0 8.1 8.2 8.3 8.4 8.5 8.6
f1 (ppm)

HSQC

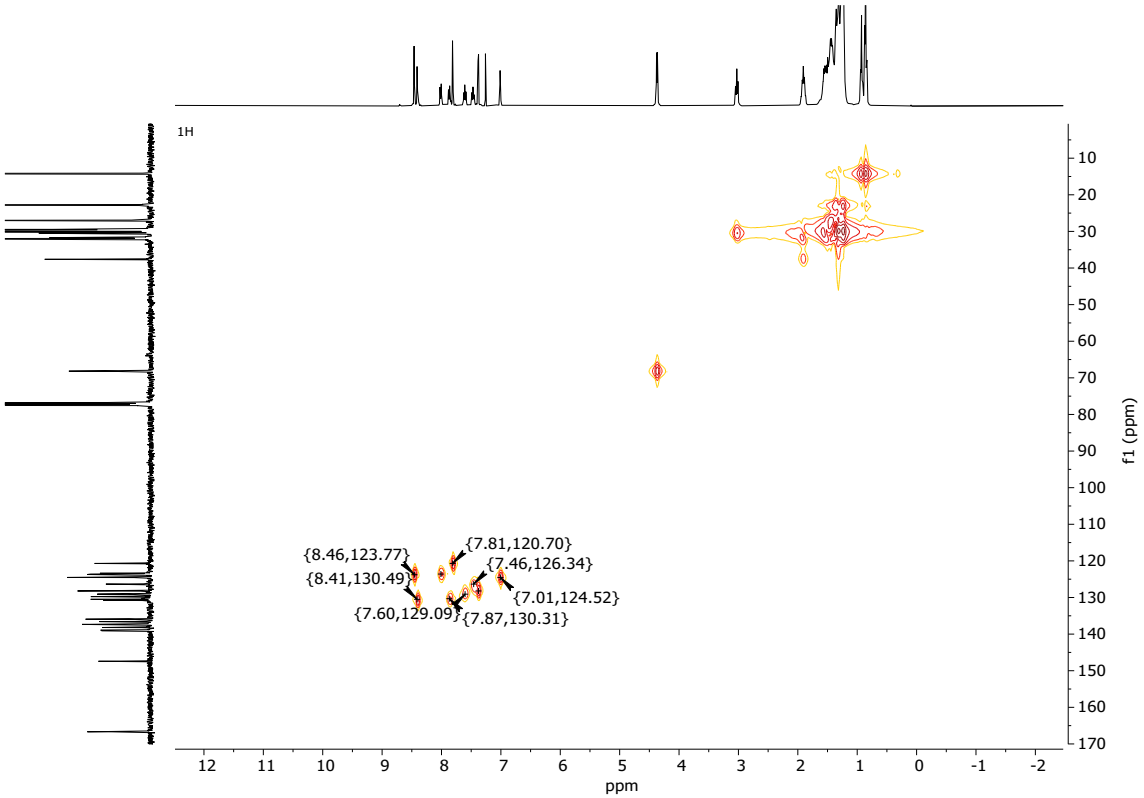
1H
{8.46,123.77}
{8.41,130.49}
{7.60,129.09}
{7.81,120.70}
{7.46,126.34}
{7.01,124.52}
{7.87,130.31}
ppm
f1 (ppm)

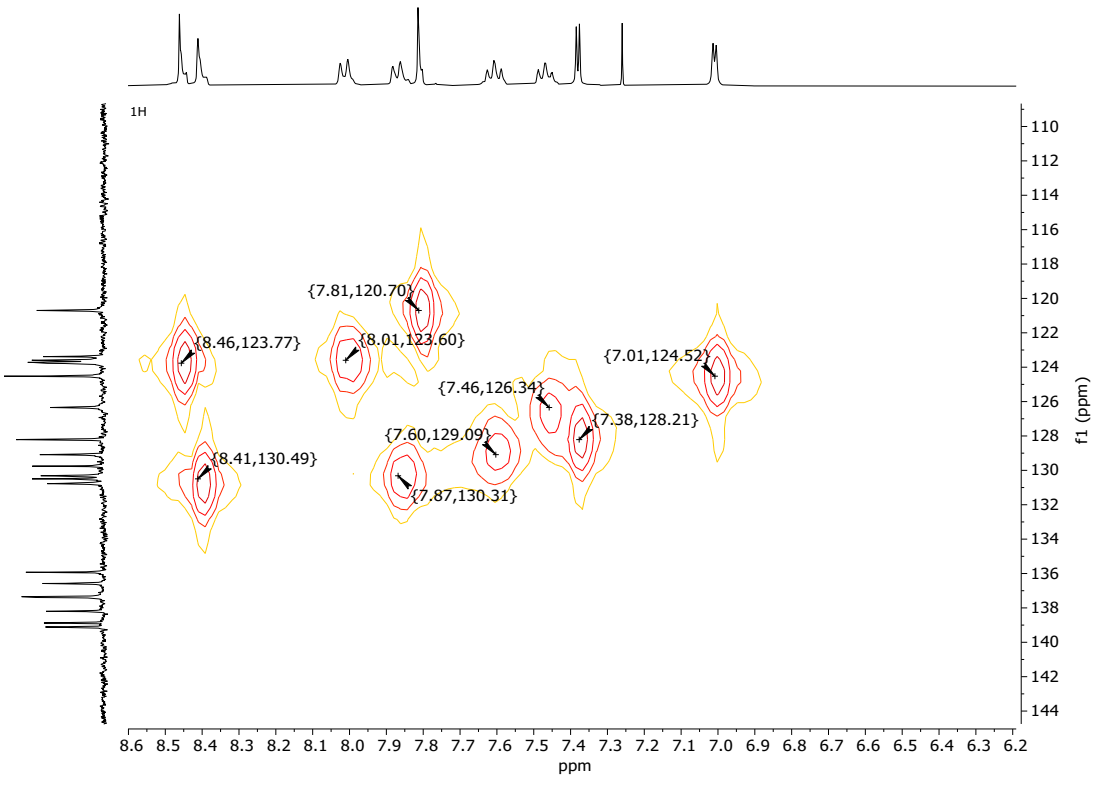
1H
{7.81,120.70}
{8.46,123.77}
{8.01,123.60}
{7.01,124.52}
{7.46,126.34}
{7.38,128.21}
{7.60,129.09}
{8.41,130.49}
{7.87,130.31}
ppm
f1 (ppm)

MALDI-TOF

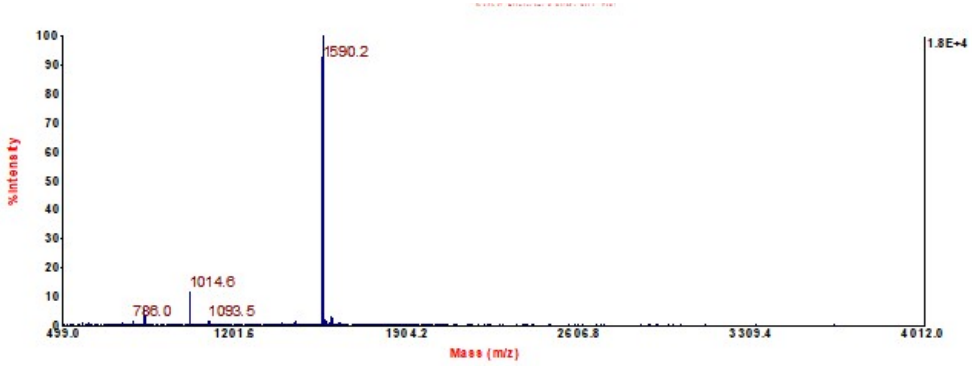

7. Additional References

(S1) Bianchi, G.; Carbonera, C.; Ciammaruchi, L.; Camaioni, N.; Negarville, N.; Tinti, F.; Forti, G.; Nitti, A.; Pasini, D.; Facchetti, A.; Pankow, R. M.; Marks, T. J.; Po, R. An Anthradithiophene Donor Polymer for Organic Solar Cells with a Good Balance between Efficiency and Synthetic Accessibility. *Solar RRL* **2022**, *6* (12), 2200643. https://doi.org/10.1002/solr.202200643.

(S2) Nitti, A.; Bianchi, G.; Po, R.; Pasini, D. Scalable Synthesis of Naphthothiophene and Benzodithiophene Scaffolds as π-Conjugated Synthons for Organic Materials. *Synthesis* **2019**, *51* (03), 677–682. https://doi.org/10.1055/s-0037-1611368.

(S3) Moreau, J. *et al.* Highly emissive nanostructured thin films of organic host–guests for energy conversion. *ChemPhysChem* **2009**, *10*, 647.

(S4) Calvi, S.; Rapisarda, M.; Valletta, A.; Scagliotti, M.; De Rosa, S.; Tortora, L.; Branchini, P.; Mariucci, L., Highly Sensitive Organic Phototransistor for Flexible Optical Detector Arrays. *Organic Electronics* **2022**, *102*, 106452.

(S5) Lim, D.-H., et al., Unsymmetrical Small Molecules for Broad-Band Photoresponse and Efficient Charge Transport in Organic Phototransistors. *ACS Applied Materials & Interfaces* **2020**, *12*, 25066-25074.

(S6) Park, J.; Kim, H.; Kim, T.; Lee, C.; Song, D.-I.; Kim, Y. Effect of Top Channel Thickness in near Infrared Organic Phototransistors with Conjugated Polymer Gate-Sensing Layers *Electronics* **2019**, DOI: 10.3390/electronics8121493.

(S7) Nam, S.; Han, H.; Seo, J.; Song, M.; Kim, H.; Anthopoulos, T. D.; McCulloch, I.; Bradley, D. D. C.; Kim, Y., Ambipolar Organic Phototransistors with P-Type/N-Type Conjugated Polymer Bulk Heterojunction Light-Sensing Layers. *Advanced Electronic Materials* **2016**, *2*, 1600264.

(S8) Zhu, M.; Lv, S.; Wang, Q.; Zhang, G.; Lu, H.; Qiu, L., Enhanced near-Infrared Photoresponse of Organic Phototransistors Based on Single-Component Donor–Acceptor Conjugated Polymer Nanowires. *Nanoscale* **2016**, *8*, 7738-7748.

(S9) Zhong, J.; Wu, X.; Lan, S.; Fang, Y.; Chen, H.; Guo, T., High Performance Flexible Organic Phototransistors with Ultrashort Channel Length. *ACS Photonics* **2018**, *5*, 3712-3722.

(S10) Wang, Q.; Zhu, M.; Wu, D.; Zhang, G.; Wang, X.; Lu, H.; Wang, X.; Qiu, L., Phototransistors Based on a Donor–Acceptor Conjugated Polymer with a High Response Speed. *Journal of Materials Chemistry C* **2015**, *3*, 10734-10741.